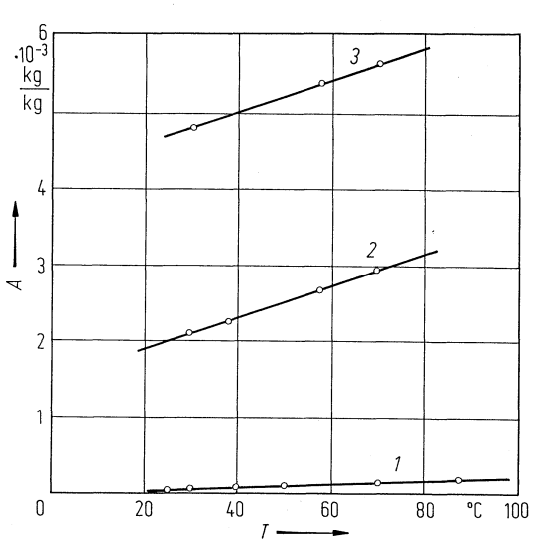

Fig. 34A-1-001. $PbHPO_4$. *A* vs. *T* for various solvents [80Bre]. *A*: solubility in acidified H_2O (kg of $PbHPO_4$ in kg solution).

Curve	Solvent
1	H_2O + 0.1 M H_3PO_4
2	H_2O + 0.05 M HNO_3
3	H_2O + 0.1 M HNO_3

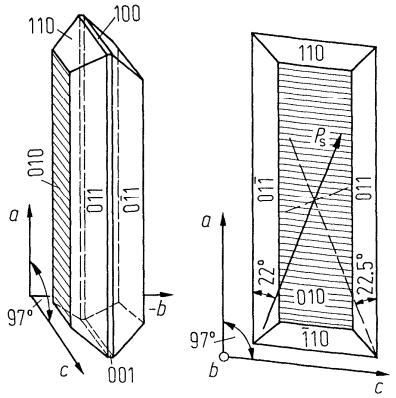

Fig. 34A-1-002. $PbHPO_4$. Crystal form grown from gel [76Bre]. Direction of P_s is shown by the arrow. Dashed lines: extinction positions under crossed Nicols.

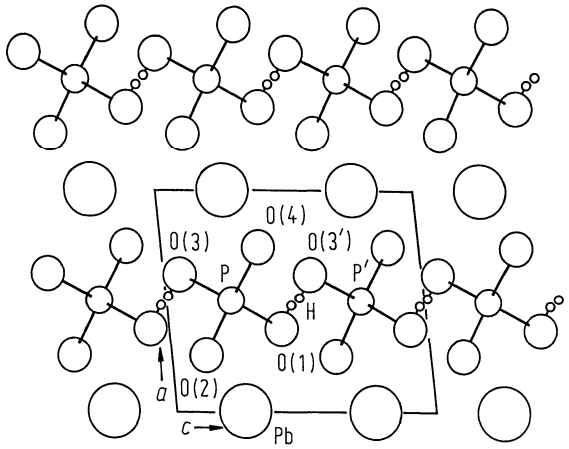

Fig. 34A-1-003. $PbHPO_4$. Crystal structure of phase I [87Res]. Projection on the (010) plane.

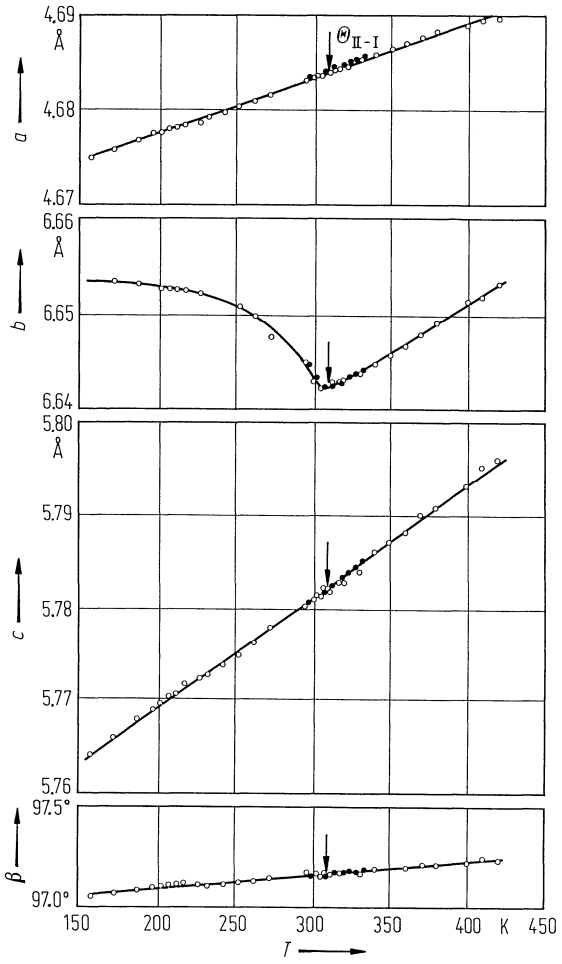

Fig. 34A-1-004. $PbHPO_4$. a, b, c, β vs. T [83Hor]. Full circles: data by [81Hor].

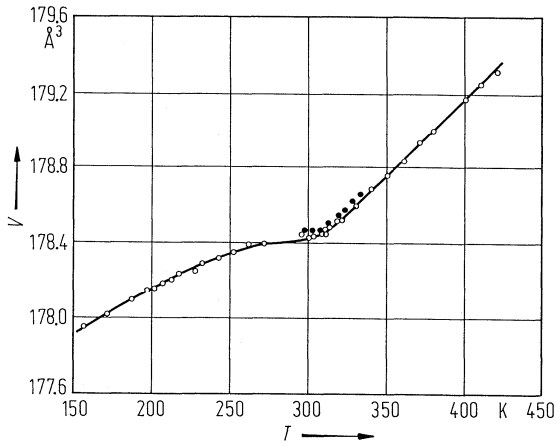

Fig. 34A-1-005. $PbHPO_4$. V vs. T [83Hor]. V: unit cell volume. Full circles: data by [81Hor].

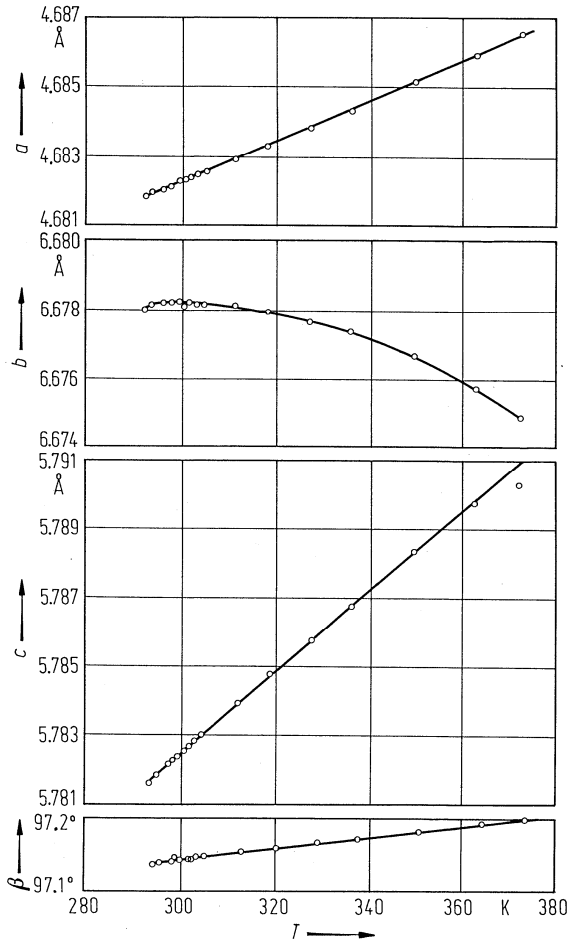

Fig. 34A-1-006. $PbDPO_4$. a, b, c, β vs. T [81Hor].

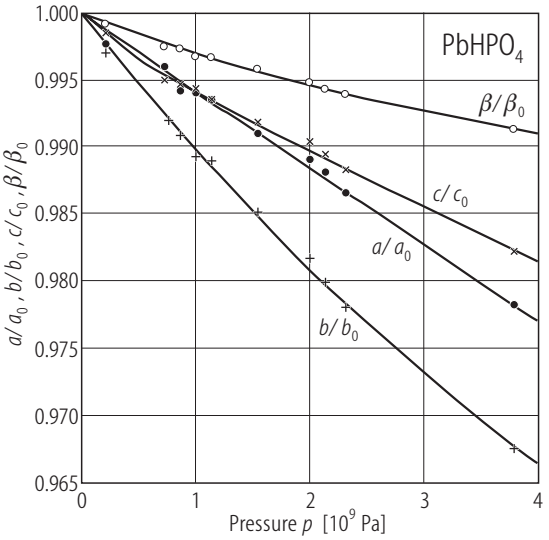

Fig. 34A-1-007. $PbHPO_4$. Relative unit cell parameters vs. p [89Kat]. T = RT.

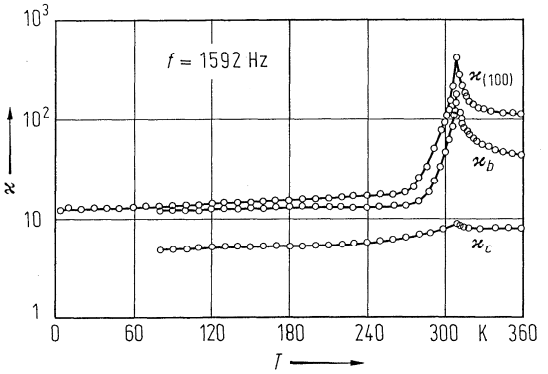

Fig. 34A-1-008. $PbHPO_4$. $\kappa_{(100)}$, κ_b, κ_c vs. T [78Smu]. $\kappa_{(100)}$: dielectric constant perpendicular to the (100) plane.

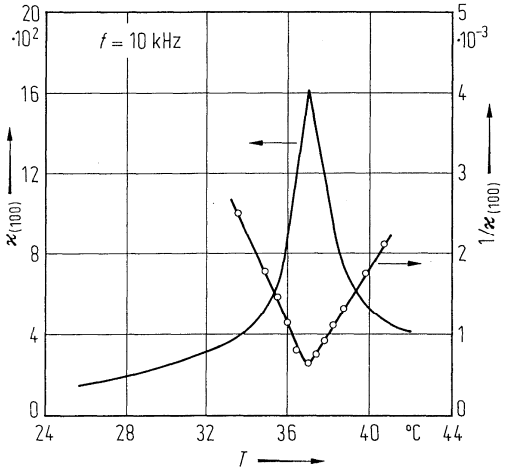

Fig. 34A-1-009. $PbHPO_4$. $\kappa_{(100)}$, $1/\kappa_{(100)}$ vs. T [74Neg]. $\kappa_{(100)}$: dielectric constant perpendicular to the (100) plane.

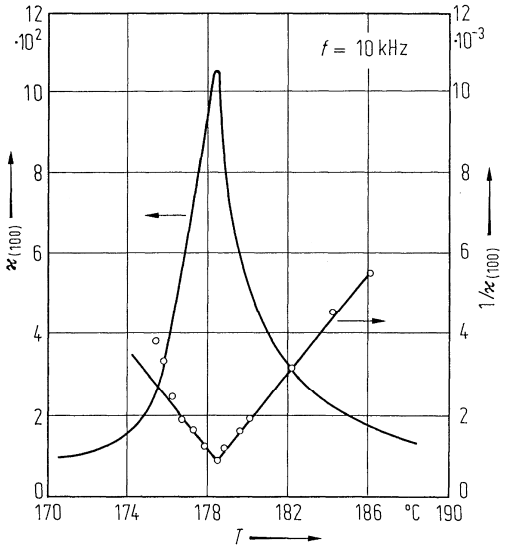

Fig. 34A-1-010. $PbDPO_4$. $\kappa_{(100)}$, $1/\kappa_{(100)}$ vs. T [74Neg]. $\kappa_{(100)}$: dielectric constant perpendicular to the (100) plane.

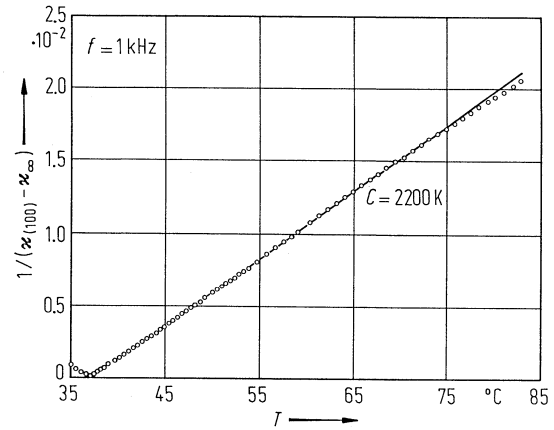

Fig. 34A-1-011. $PbHPO_4$. $1/(\kappa_{(100)} - \kappa_\infty)$ vs. T [88Deg]. $\kappa_{(100)}$: dielectric constant perpendicular to the (100) plane. $\kappa_\infty = 10$.

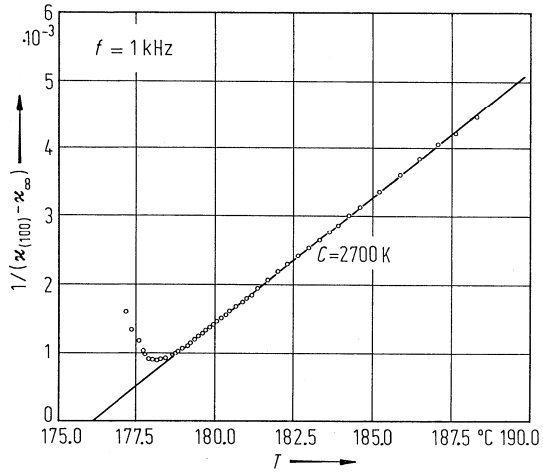

Fig. 34A-1-012. $PbDPO_4$. $1/(\kappa_{(100)} - \kappa_\infty)$ vs. T [88Deg]. $\kappa_{(100)}$: dielectric constant perpendicular to the (100) plane. $\kappa_\infty = 10$.

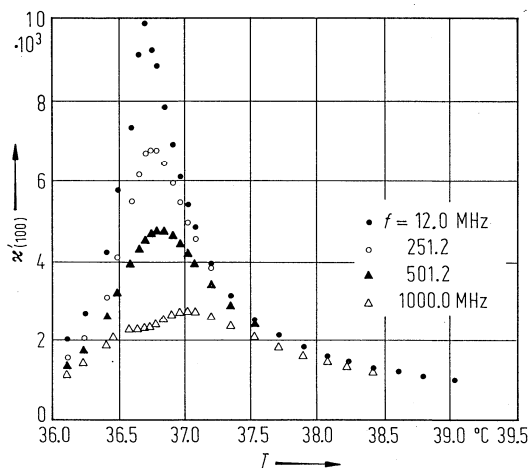

Fig. 34A-1-013. $PbHPO_4$. $\kappa'_{(100)}$ vs. T [88Deg]. Parameter: f. $\kappa'_{(100)}$: real part of dielectric constant perpendicular to the (100) plane.

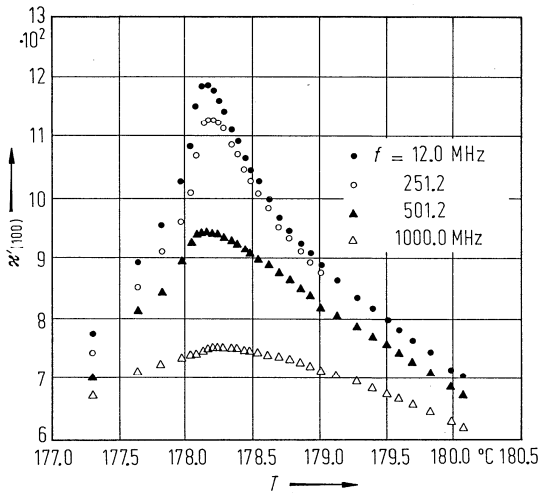

Fig. 34A-1-014. $PbDPO_4$. $\kappa'_{(100)}$ vs. T [88Deg]. Parameter: f. $\kappa'_{(100)}$: real part of dielectric constant perpendicular to the (100) plane.

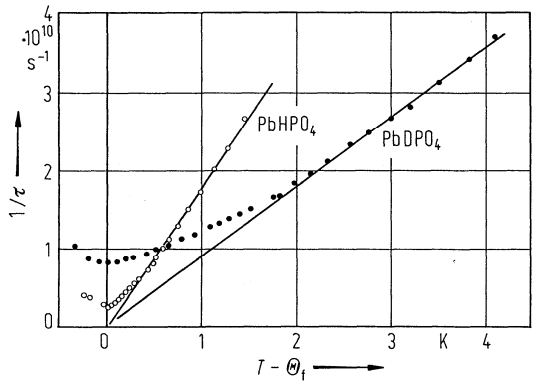

Fig. 34A-1-015. $PbHPO_4$, $PbDPO_4$. $1/\tau$ vs. $T - \Theta_f$ [88Deg]. τ: dielectric relaxation time.

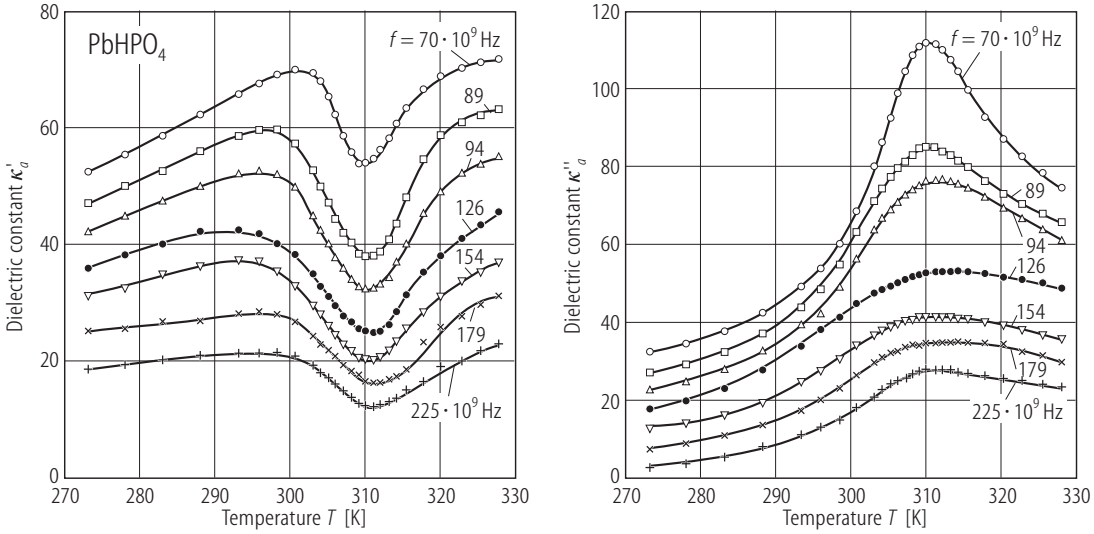

Fig. 34A-1-016. $PbHPO_4$. κ_a', κ_a'' vs. T [92Bri]. Parameter: f. The scale refers to the curves at 225 GHz. The upper curves are shifted by a multiple of five units.

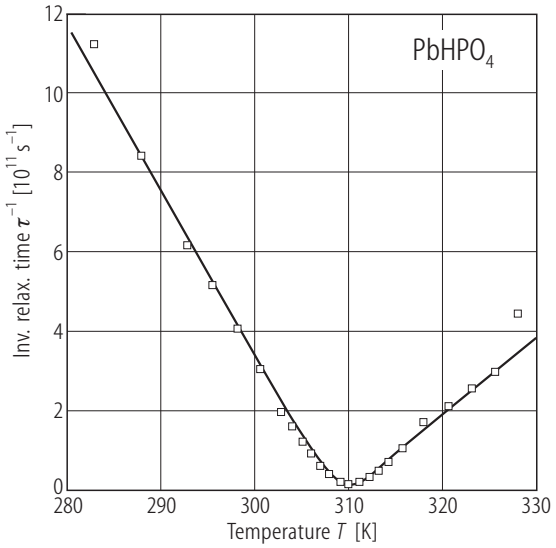

Fig. 34A-1-017. $PbHPO_4$. $1/\tau$ vs. T [92Bri]. τ: dielectric relaxation time obtained by millimeter wave measurements.

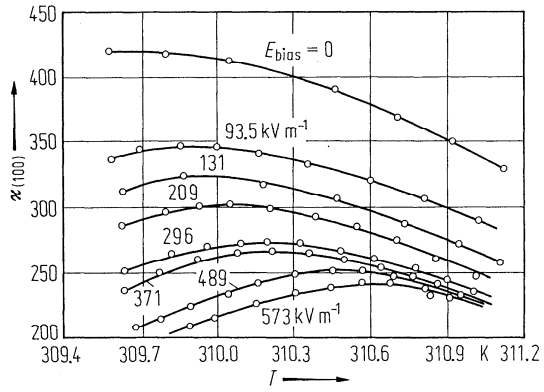

Fig. 34A-1-018. $PbHPO_4$. $\varkappa_{(100)}$ vs. T [78Smu]. Parameter: E_{bias}. $\varkappa_{(100)}$: real part of dielectric constant perpendicular to the (100) plane. f = 1592 Hz.

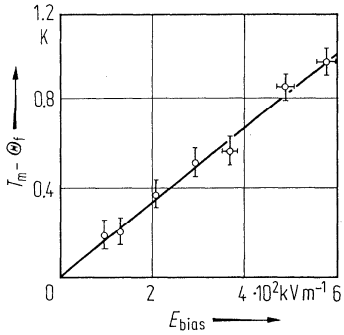

Fig. 34A-1-019. $PbHPO_4$. $T_m - \Theta_f$ vs. E_{bias} [78Smu]. T_m: temperature at which $\varkappa_{(100)}$ is maximum.

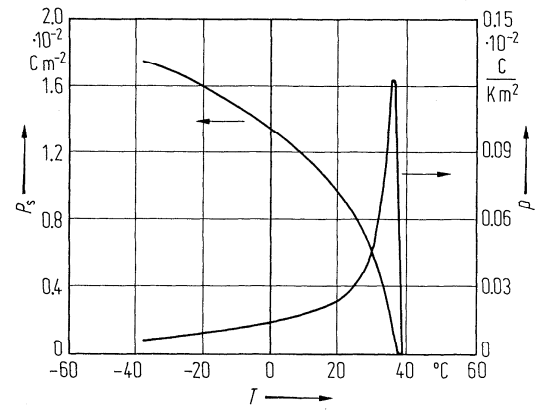

Fig. 34A-1-020. $PbHPO_4$. P_s, p vs. T measured on (100) plate specimen [74Neg]. $p = dP_s/dT$: pyroelectric coefficient.

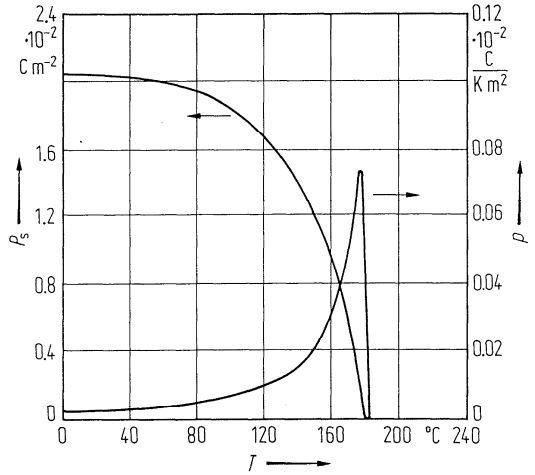

Fig. 34A-1-021. $PbDPO_4$. P_s, p vs. T measured on (100) plate specimen [74Neg]. $p = dP_s/dT$: pyroelectric coefficient.

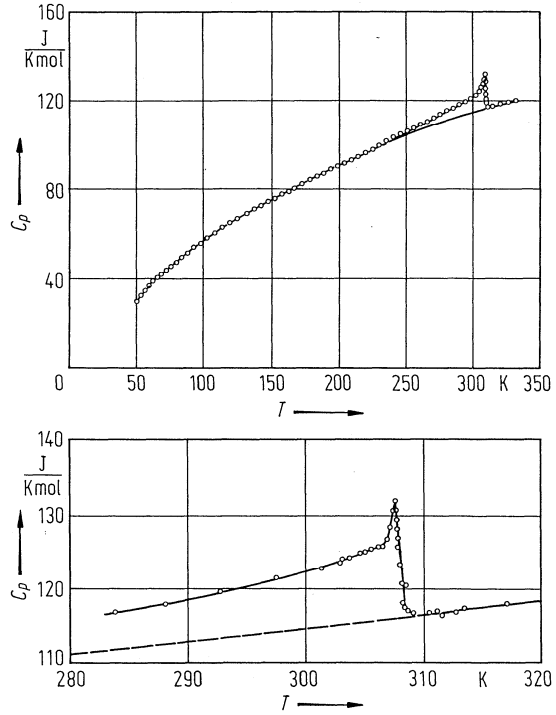

Fig. 34A-1-022. $PbHPO_4$. C_p vs. T [81Lop].

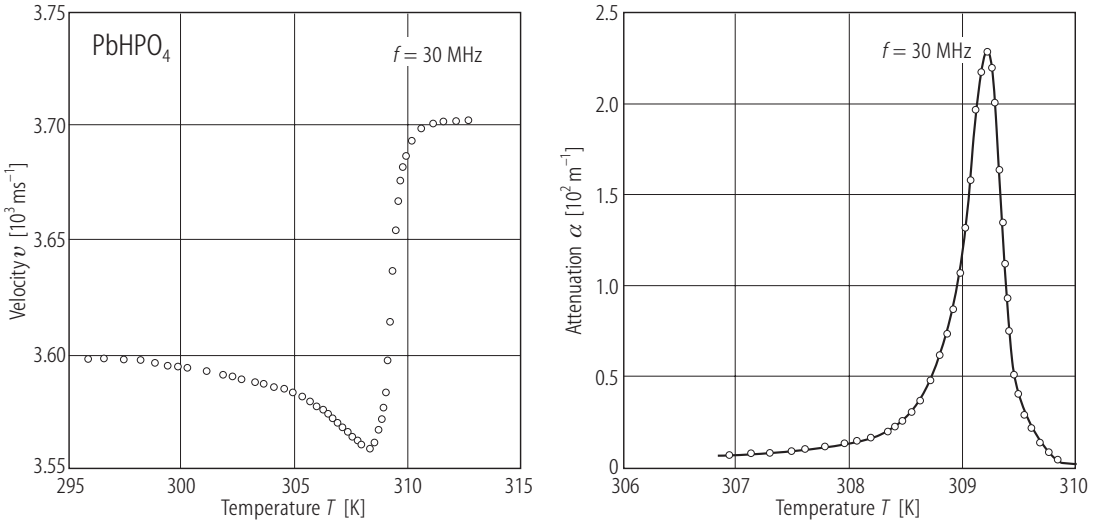

Fig. 34A-1-023. $PbHPO_4$. υ, α vs. T [94Miz]. υ, α: velocity and attenuation of longitudinal ultrasonic wave propagating along the *c* axis.

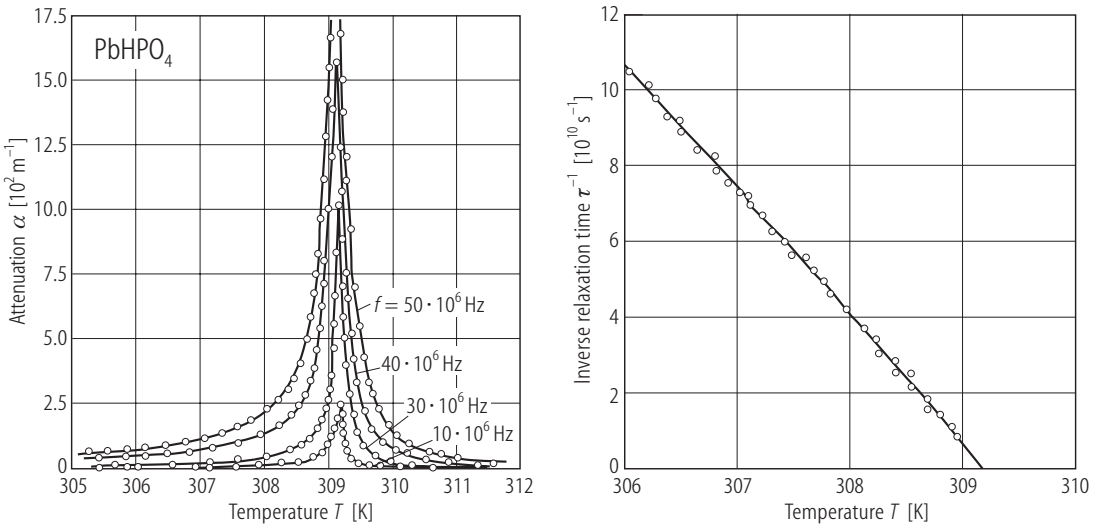

Fig. 34A-1-024. $PbHPO_4$. α, $1/\tau$ vs. T [94Miz]. Parameter: *f*. α: attenuation of longitudinal ultrasonic wave propagating along the *b* axis. τ: ultrasonic relaxation time.

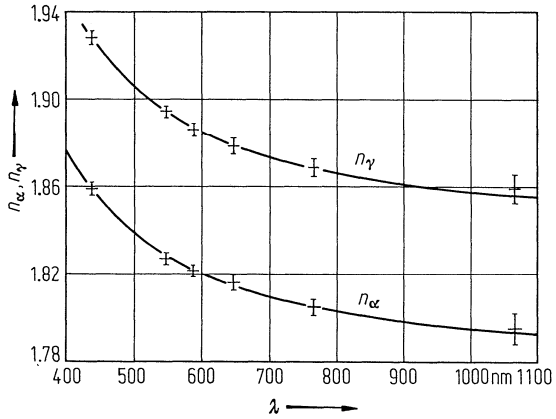

Fig. 34A-1-025. $PbHPO_4$. n_α, n_γ vs. λ [88Kee]. $n_\beta = n_\alpha$ within accuracy of measurement.

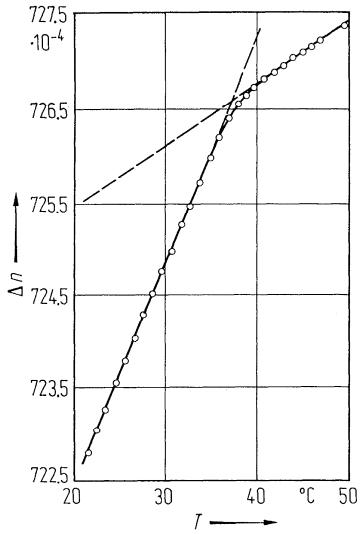

Fig. 34A-1-026. $PbHPO_4$. Δn vs. T [77Kon]. $\Delta n = n_\gamma - n_\beta$. $\lambda = 633$ nm.

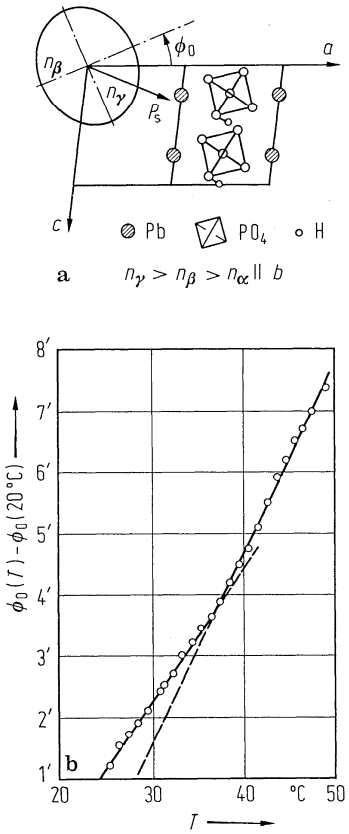

Fig. 34A-1-027. $PbHPO_4$. (**a**) The orientation of indicatrix and P_s referring to the crystal structure. (**b**) $\phi_0(T) - \phi_0(20\ °C)$ vs. T [78Kon]. $\phi_0(T)$: angle of indicatrix at T.

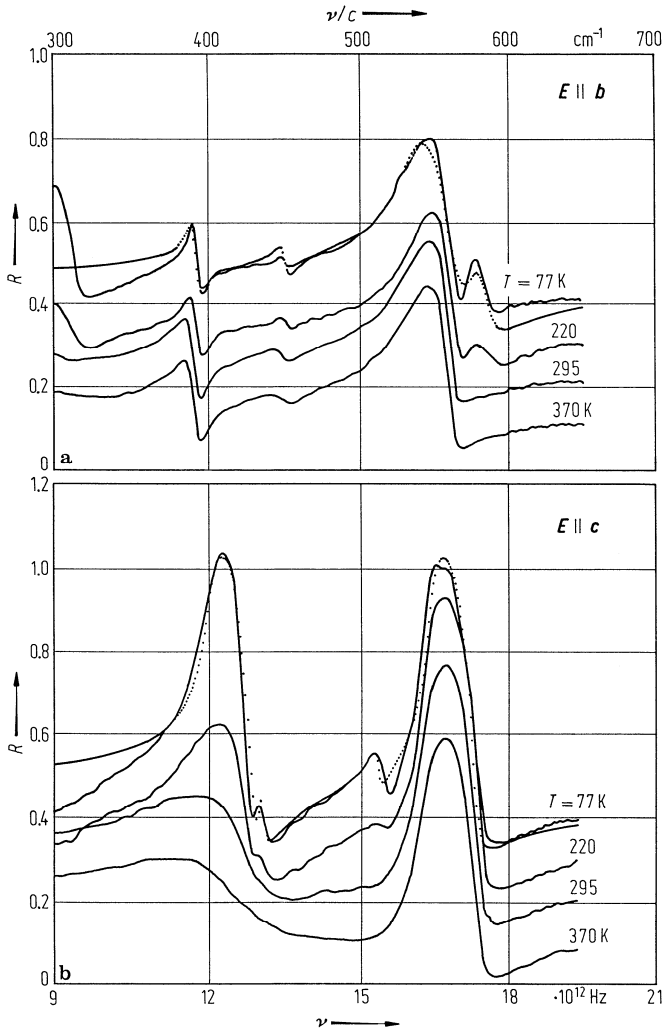

Fig. 34A-1-028. $PbHPO_4$. R vs. ν [85Hap]. Parameter: T. R: reflectivity, ν: frequency of incident infrared radiation. (**a**) $\boldsymbol{E} \parallel \boldsymbol{b}$, (**b**) $\boldsymbol{E} \parallel \boldsymbol{c}$. Dotted lines for 77 K are the oscillator fit. The lines are shifted by 0.1 relative to each other.

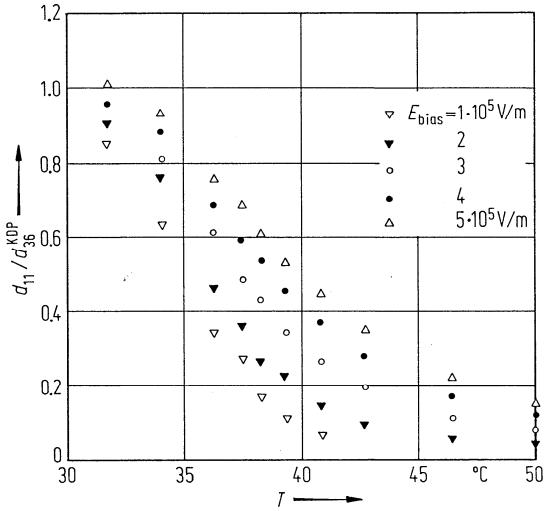

Fig. 34A-1-029. $PbHPO_4$. d_{11}/d_{36}^{KDP} vs. T [87Zgo]. Parameter: E_{bias}. $d_{i\lambda}$: susceptibility for second harmonic generation. $\lambda = 1.06$ μm.

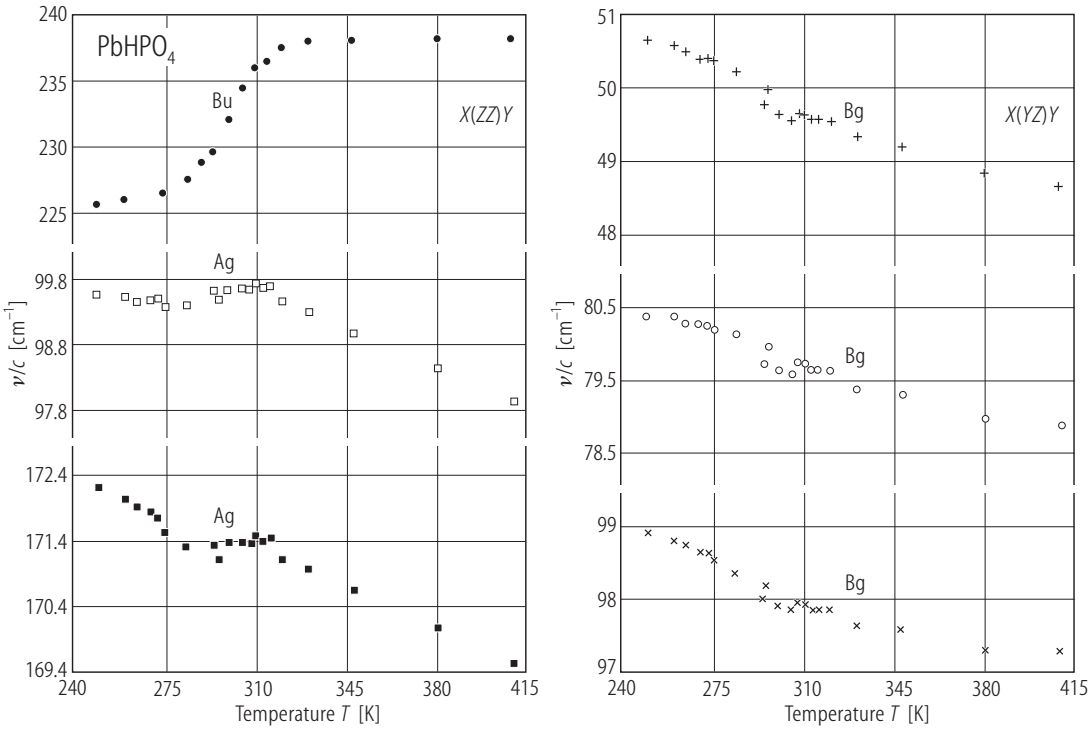

Fig. 34A-1-030. $PbHPO_4$. ν/c vs. T [87Loc]. ν: Raman frequency due to lattice modes. $X \parallel a$, $Y \parallel b$, $Z \parallel c^*$.

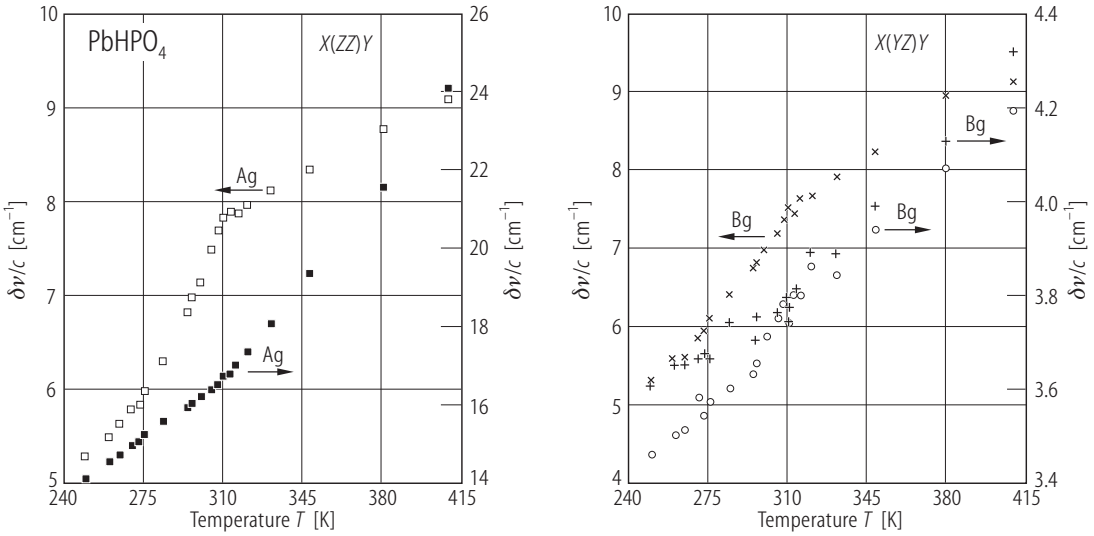

Fig. 34A-1-031. $PbHPO_4$. $\delta\nu/c$ vs. T [87Loc]. $\delta\nu$: line width of Raman scattering due to lattice modes. $X \parallel a$, $Y \parallel b$, $Z \parallel c^*$. Marks correspond to those in Fig. 34A-1-030.

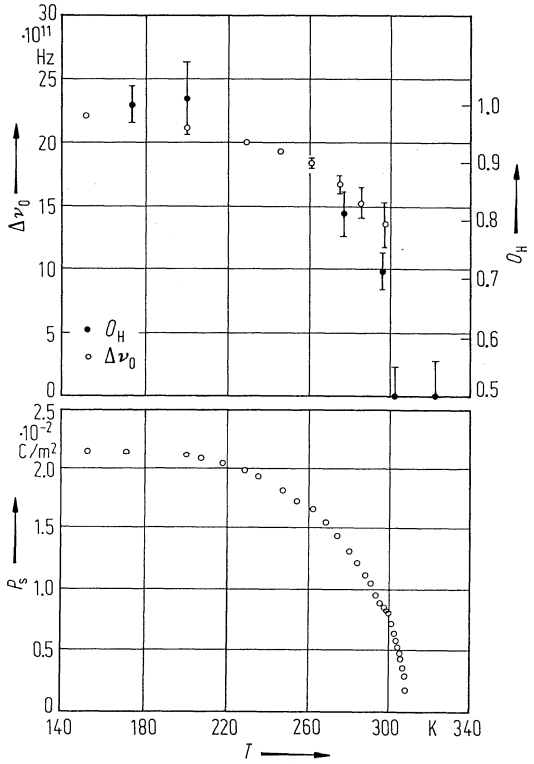

Fig. 34A-1-032. $PbHPO_4$. $\Delta\nu_0$, P_s vs. T [85Loc]. $\Delta\nu_0$: Raman shift of the soft mode. In upper figure, full circle: hydrogen ordering, O_H, obtained from neutron scattering [85Nel].

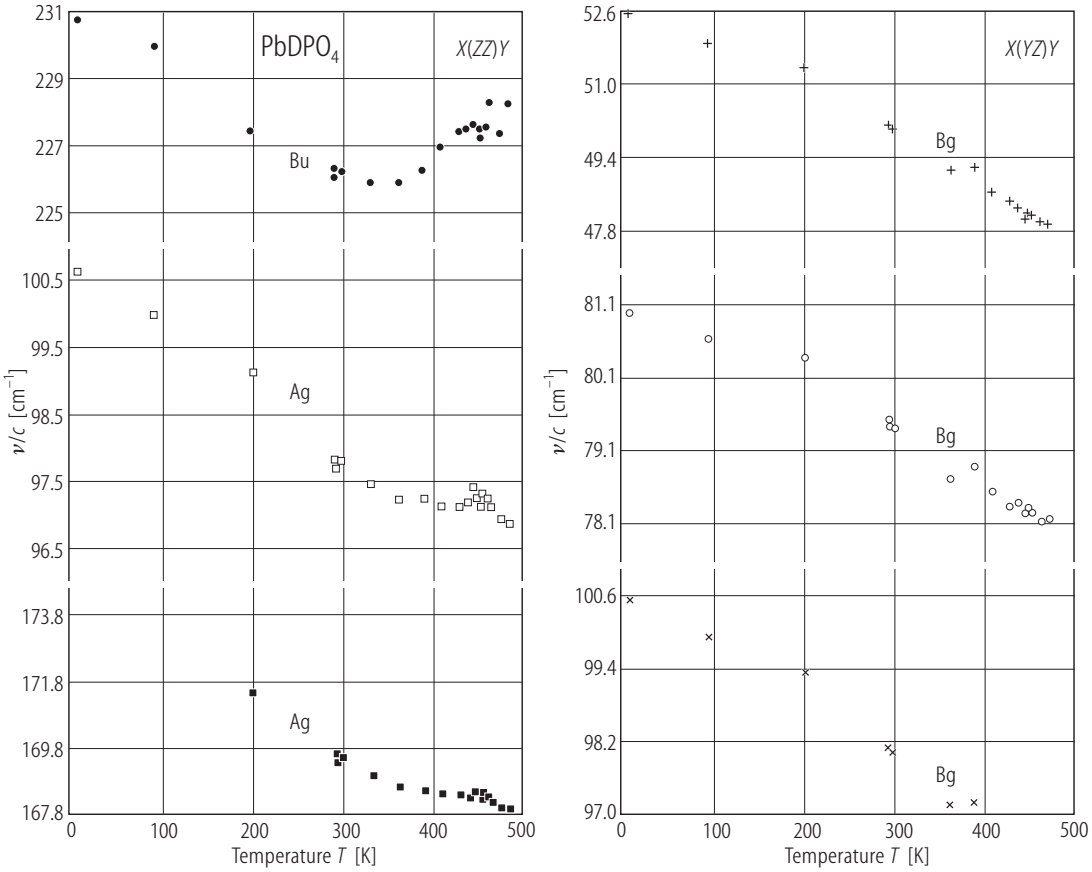

Fig. 34A-1-033. $PbDPO_4$. ν/c vs. T [87Ohn]. ν: Raman scattering frequency due to lattice modes. $X \parallel a$, $Y \parallel b$, $Z \parallel c^*$.

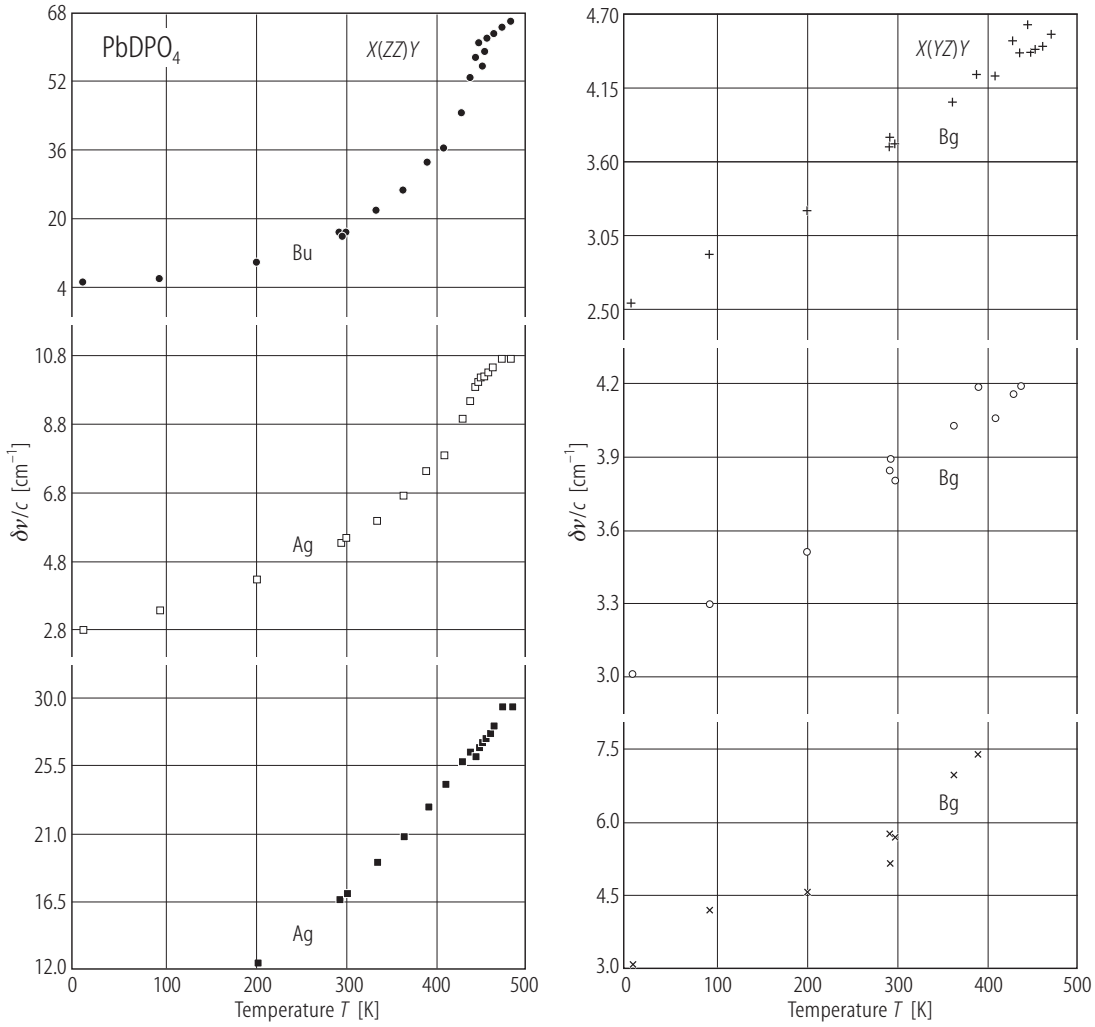

Fig. 34A-1-034. $PbDPO_4$. $\delta\nu/c$ vs. T [87Ohn]. $\delta\nu$: line width of Raman scattering due to lattice modes. $X \parallel a$, $Y \parallel b$, $Z \parallel c^*$.

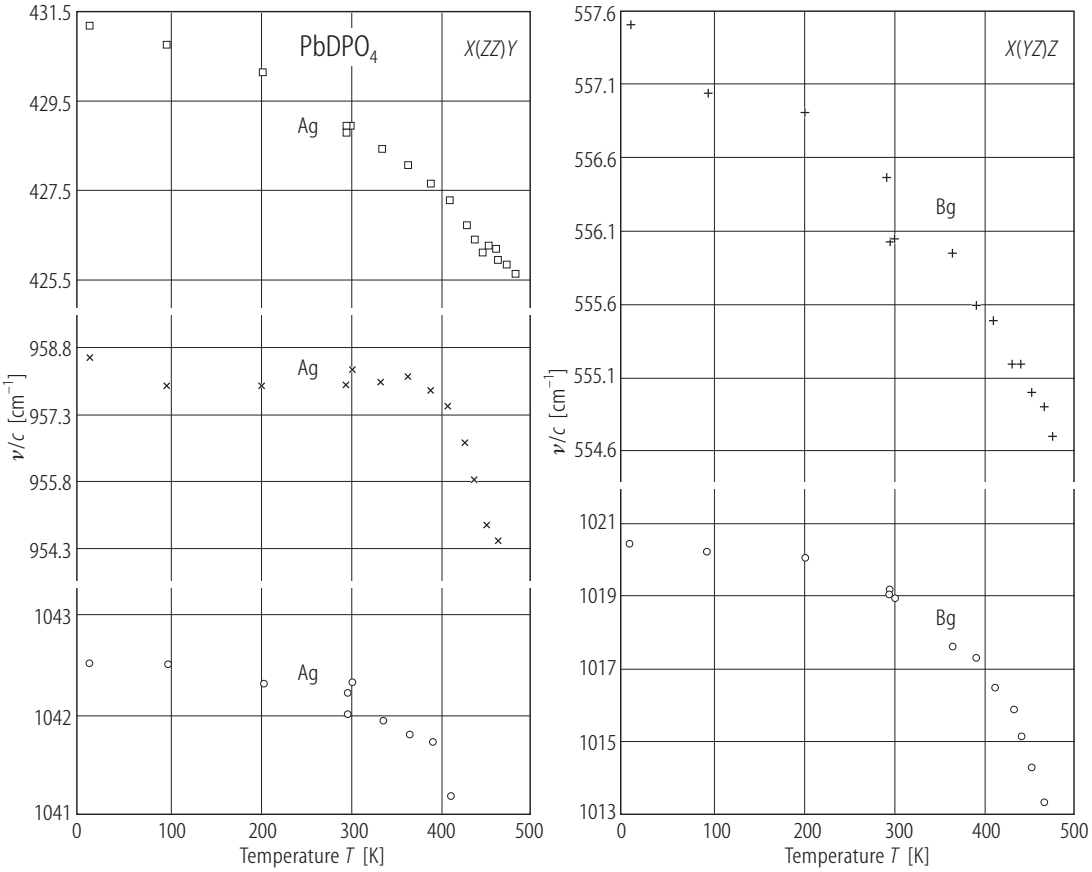

Fig. 34A-1-035. $PbDPO_4$. ν/c vs. T [87Ohn]. ν: Raman frequency due to PO_4 internal modes. $X \parallel a$, $Y \parallel b$, $Z \parallel c^*$.

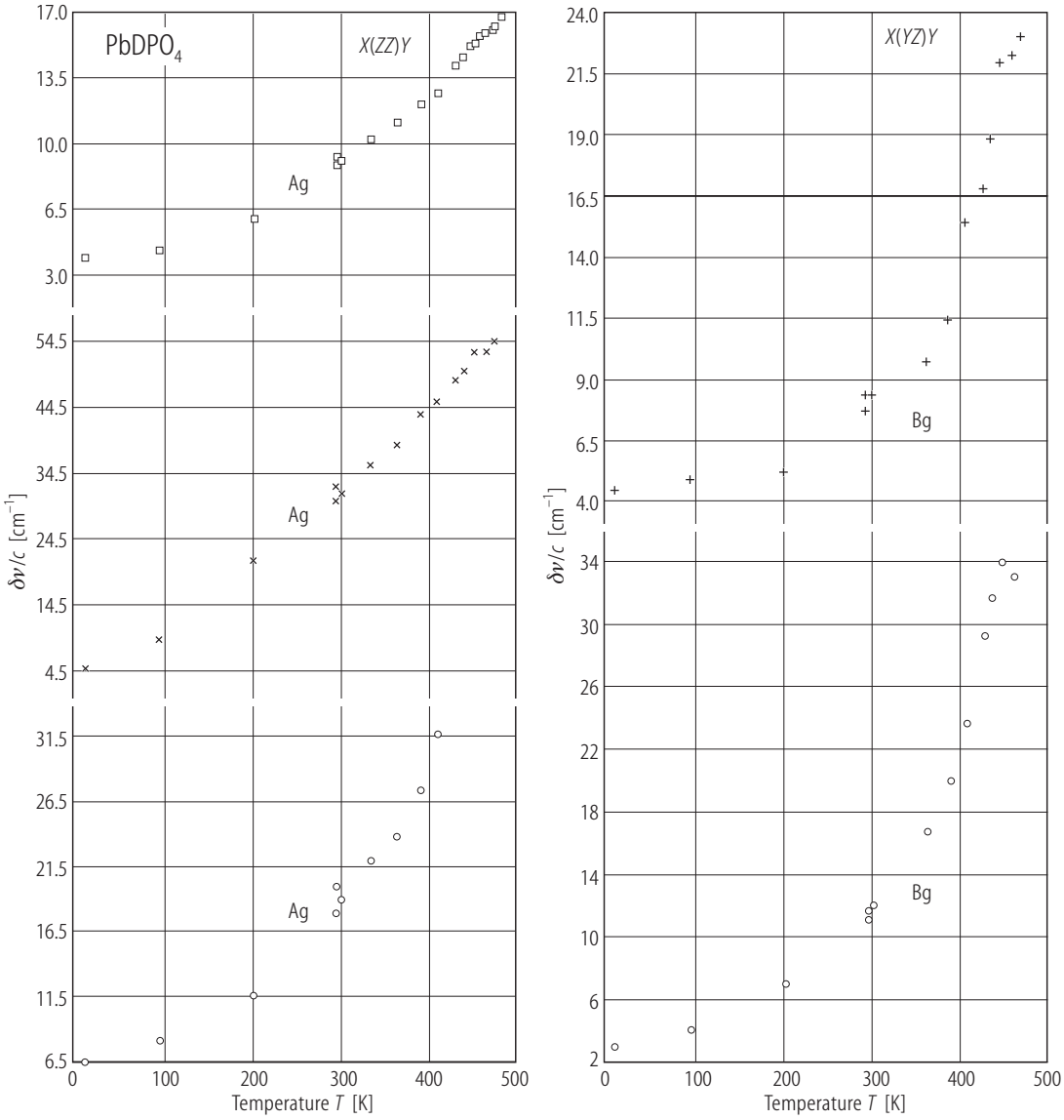

Fig. 34A-1-036. $PbDPO_4$. $\delta\nu/c$ vs. T [87Ohn]. $\delta\nu$: line width of Raman scattering due to PO_4 internal modes. $X \parallel a$, $Y \parallel b$, $Z \parallel c^*$.

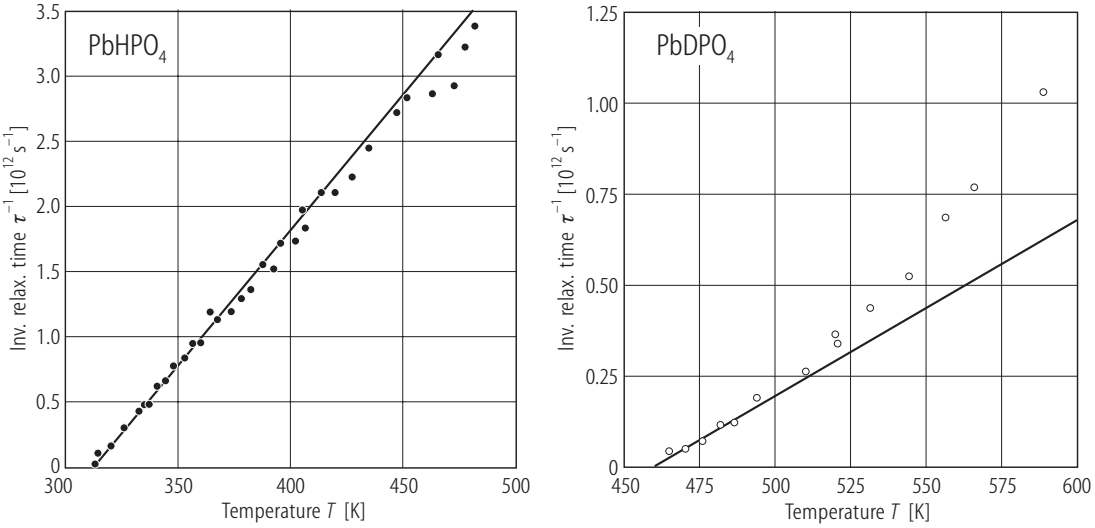

Fig. 34A-1-037. $PbHPO_4$, $PbDPO_4$. $1/\tau$ vs. T [90Shi]. τ: relaxation time measured by hyper-Raman scattering.

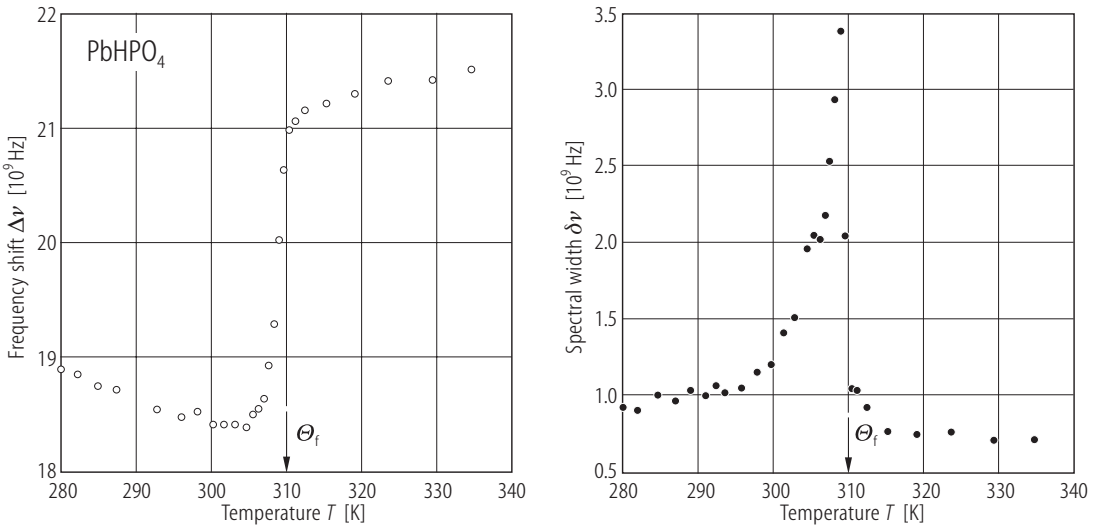

Fig. 34A-1-038. $PbHPO_4$. $\Delta\nu$, $\delta\nu$ vs. T [92Luz]. $\Delta\nu$, $\delta\nu$: frequency shift and line width of Brillouin scattering corresponding to pure longitudinal c_{22} mode propagating along the b axis.

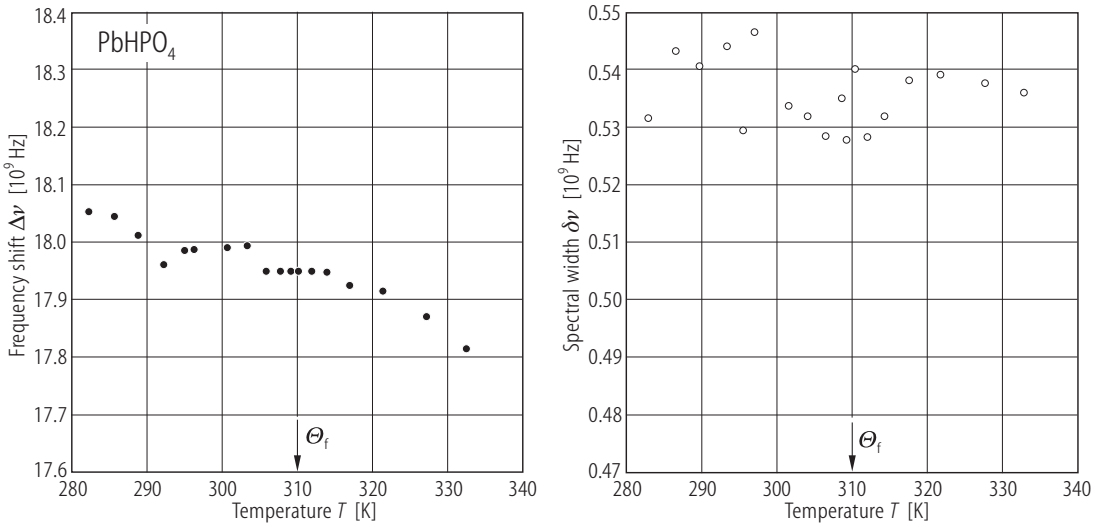

Fig. 34A-1-039. $PbHPO_4$. $\Delta\nu$, $\delta\nu$ vs. T [92Luz]. $\Delta\nu$, $\delta\nu$: frequency shift and line width of Brillouin scattering corresponding to quasi-longitudinal mode propagating along the a^* axis.

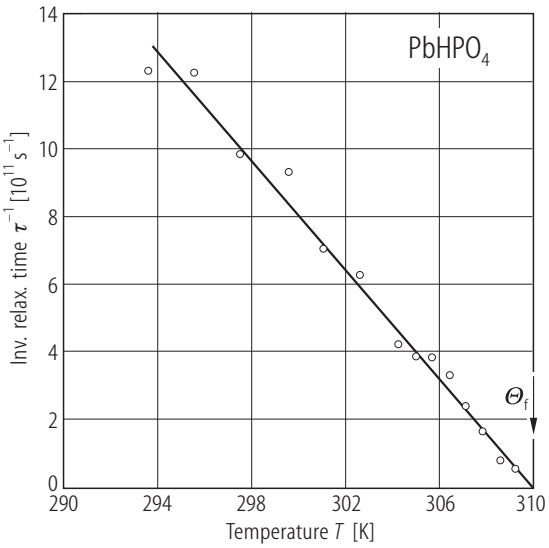

Fig. 34A-1-040. $PbHPO_4$. $1/\tau$ vs. T [92Luz]. τ: relaxation time of polarization fluctuation obtained by line width measurements of Brillouin scattering.

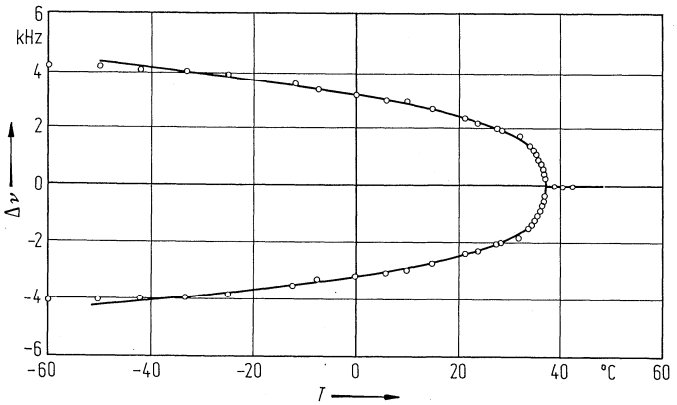

Fig. 34A-1-041. $PbHPO_4$. $\Delta\nu$ vs. T [86Top]. $\Delta\nu$: ^{207}Pb NMR line splitting. H is in the (001) plane making an angle 120° with the a axis.

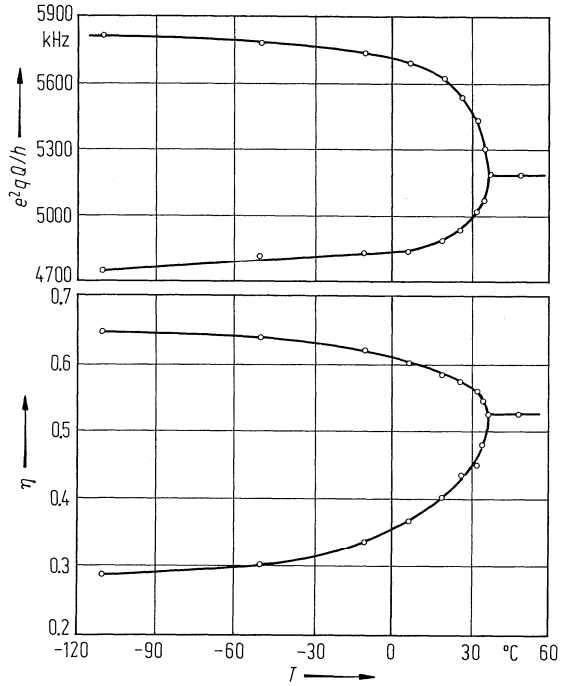

Fig. 34A-1-042. $PbHPO_4$. e^2qQ/h, η vs. T [83Sel]. e^2qQ/h: nuclear quadrupole coupling constant of ^{17}O, η: asymmetry parameter.